Hindawi
International Journal of RF and Microwave Computer-Aided Engineering
Volume 2023, Article ID 6610220, 10 pages
https://doi.org/10.1155/2023/6610220

Research Article

Demonstration of a Wideband Multipolarization Transmitarray Antenna for Satellite Communication

Luming Zhang, Hao Jiang, Yihang Li, Yixin Suo, Fan Yang, Feiliang Chen, Mo Li, Qiye Wen, and Jian Zhang

School of Electronic Science and Engineering, University of Electronic Science and Technology of China, 611731 Chengdu, Sichuan, China

Correspondence should be addressed to Jian Zhang; jianzhang@uestc.edu.cn

Received 30 November 2022; Revised 10 January 2023; Accepted 20 April 2023; Published 8 May 2023

Academic Editor: Arpan Desai

To meet the requirements of satellite communication (SATCOM), in this paper, a wideband high stability transmitarray antenna (TA) for SATCOM is proposed. The TA is composed of 225 metal-only unit cells that comprise three metallic layers with an air spacer in between. High stability is capable by adopting a simple metallic square loop and two pairs of orthogonal stubs with a 1 mm thickness of the layer, which ensures lower assembly complexity and higher integration. The proposed unit cell can also support linear polarization (LP) wave excitation and circular polarization (CP) wave excitation simultaneously. Meanwhile, the metal-only unit cell can operate without dielectric loss, which leads to higher working efficiency. By adjusting feature sizes, eight different kinds of the unit cell are designed to realize a 3-bit TA which enables obtaining a gain of 23.53 dBi. Finally, four TA prototypes have been fabricated and tested successfully. The measured result shows a 28.5% 3 dB gain bandwidth from 30 GHz to 40 GHz, which is in good consistency with the simulated design. This compact and mechanical robustness design provides an alternative proposal for SATCOM.

1. Introduction

With the rapid development of SATCOM [1–6], the trend of broadband wireless applications in the millimeter wave band (Ka-band) is rising in the research community. Ka-band spectrum resources are abundant to provide a means of new services for a high data rate in SATCOM. As an indispensable technology method in broadband wireless applications, the transmitarray antenna (TA) plays an important role in the field of modern wireless communication. It can replace the traditional parabolic antenna and phased array antenna [7] for more convenient and efficient transmission in many environments.

In the past few years, there have been many types of research and reports on TA. By combining the advantages of the flat lens and phased array antenna, TA has the characteristics of a simple structure and low processing cost. Based on the traditional PCB technology, there are some relevant TA designs in various frequency bands [8–18]. Numerous applications of the traditional PCB technology TA design in communication are proposed. Among them, the metal-only TA configuration has been released and provided many performance advantages [19–28]. After doing full investigations, we got a comprehensive analysis of the state-of-the-art developments in the metal-only TAs. A high-efficient metal-only TA with a quad metal layer was presented in [20] for space application, and a 23.76 dB gain at 11.3 GHz was achieved. In [22], the TA with varied element thickness was proposed with 24.27% 1 dB gain bandwidth and 62% aperture efficiency. In [25], a TA based on a C-shaped slot element can realize an 11% 3 dB gain bandwidth in Ka-band with 50% aperture efficiency. In [27], a wideband metal-only TA with a two-layer configuration was reported. It showed that the TA can realize 14.6% 1 dB gain bandwidth and 47.6% aperture efficiency at 8.5 GHz. As an efficient transmission design scheme, the metal-only structure was feasible and practical. The metal-only designs reported above were mostly in the field of low-frequency applications,

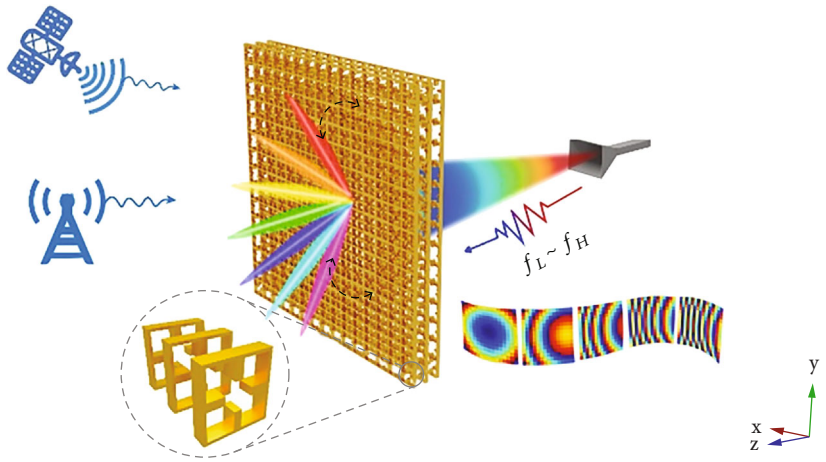

FIGURE 1: Conceptual architecture of the proposed metal-only transmitarray antenna and its application background.

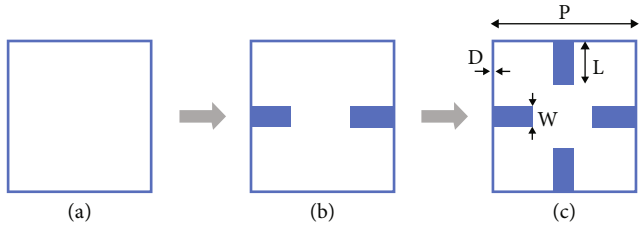

FIGURE 2: Schematic of the proposed single metal-only unit cell. (a) Square loop. (b) Square loop with a pair of stubs. (c) Square loop with two pairs of orthogonal stubs.

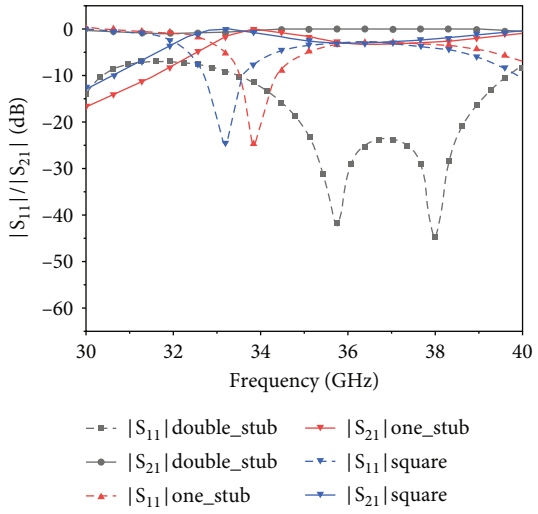

FIGURE 3: The simulated S_{21} magnitude and S_{11} magnitude of three kinds of the unit cell with three metallic layers.

which cannot fully utilize the advantages of the metal-only structures in high-frequency bands. In addition, the existing metal-only TA polarization excitation modes are single, most of which are line polarization excitation modes, and the working bandwidth is narrow. Few achievements can be applied to the whole Ka-band.

In this paper, we proposed a unit cell with a square loop and two pairs of orthogonal stubs. The overall structure of the unit cell is simple, and the metallic material is mechanically strong and chemically stable; hence, it has strong stability in complex space working environments. Meanwhile, the unit cell can support linear polarization (LP) wave excitation and circular polarization (CP) wave excitation simultaneously, which is suitable for SATCOM. The proposed TA has a 3 dB bandwidth of 28.5%. By adjusting some feature sizes, we can get eight different kinds of unit cells to realize the 3-bit TA design. Multibit unit cell design enables the TA to obtain higher gain. The beam steering direction of the TAs can be determined by calculating phase compensation values in different positions of the transmitarray. The conceptual architecture of the proposed metal-only TA and its application background can be seen in Figure 1.

This paper is organized as follows. The detailed geometry and the principle of the unit cell are presented in Section 2. In Section 3, we present the TA configuration based on the metal-only unit cell and provide the simulated and measured results. Section 4 shows the fabrication and measurements. Conclusions are drawn in Section 5.

2. Design of the Metal-Only Unit Cell

In this section, the design of the unit cell (UC) is introduced. The unit cell configuration design has evolved in two stages, which can be seen in Figure 2. The periodicity of the unit is $P = 4.3$ mm, which is around half the wavelength at the central operating frequency of 35 GHz. And the width of the stub, $W = 0.5$ mm, is fixed. The material of the metal layers is brass with a conductivity of 1.5×10^7 S/m. As shown in Figure 3, three kinds of metal-only unit cells are simulated by the frequency-domain solver of CST microwave studio with the unit cell boundary condition. The square loop structure has a certain passband response in the working frequency band. Its transmission magnitude satisfies the requirements in a narrow bandwidth. The passband transmission coefficient of the unit cell can be changed by adding a pair of parallel variable stubs. To further improve the broadband performance of the unit cell, another pair of orthogonal stubs is introduced. These stubs bring additional low-frequency resonance, which can form a wide passband

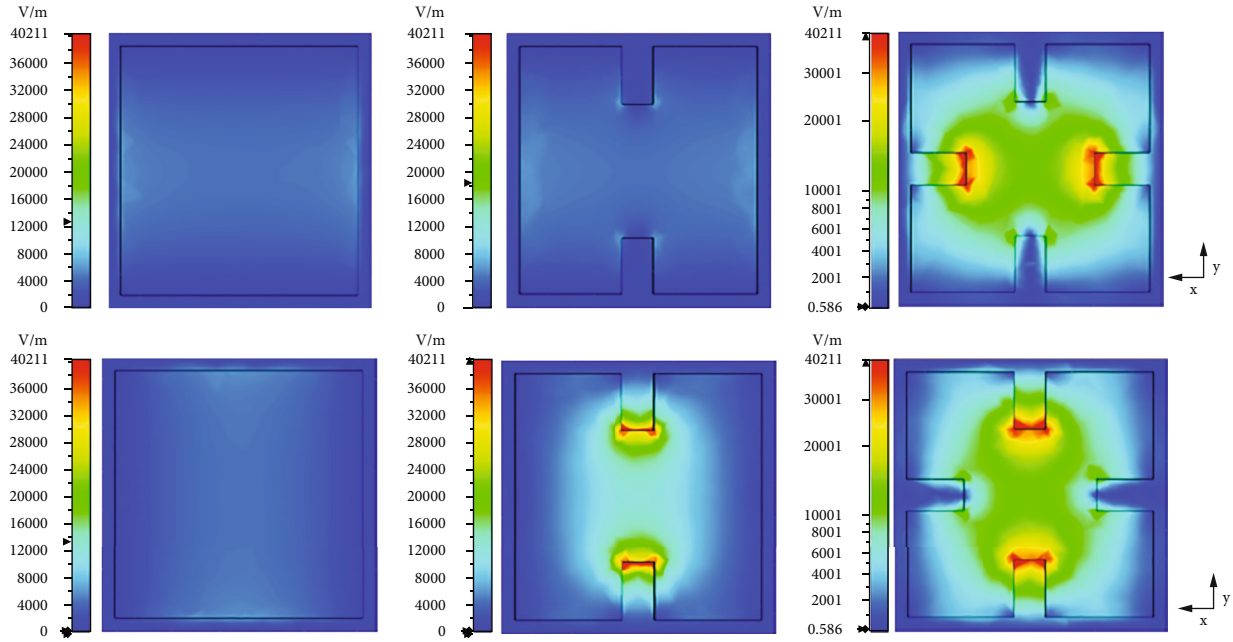

Figure 4: The simulated E field intensity of three kinds of the unit cell with two polarization directions.

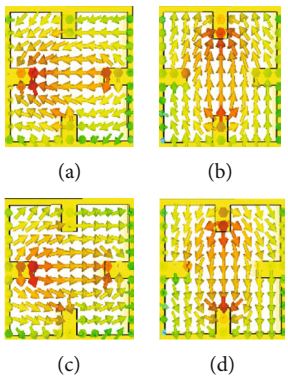

Figure 5: The simulated electric field inside the metal-only unit cell as it progresses overphase. The electric field phase changes from (a) 0°, (b) 90°, (c) 180°, to (d) 270°.

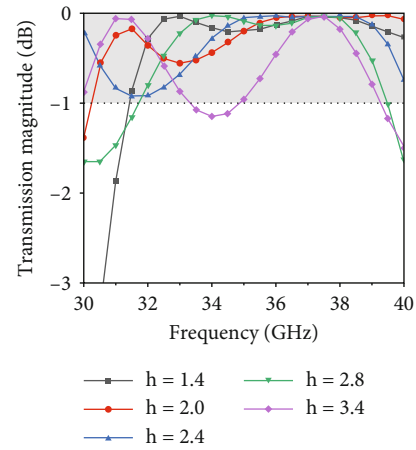

Figure 6: Simulated transmission magnitudes of the UC2 with different h values.

Table 1: Geometric parameters of the metal-only unit cell.

No. of UC	L (mm)	D (mm)
UC1	1.3	0.2
UC2	1.4	0.25
UC3	0.7	0.35
UC4	0.6	0.3
UC5	0.7	0.25
UC6	0.9	0.2
UC7	1.1	0.2
UC8	1.4	0.4

response together with the resonance of the unit cell. Meanwhile, two pairs of orthogonal stubs will also interact to form a new resonance.

In Figure 4, we have analyzed the electric field resonance for the three cases in Figure 3. When the incident electric field polarization direction is along the x-axis or y-axis, we selected the cases corresponding to the highest electric field intensity in the three kinds of unit cells. For the square loop unit cell, due to its symmetrical structure, the resonance effect generated by the electric field in both excitation directions when passing through the unit cell is the same, and the highest intensity is 13049 V/m. For the single-stub unit cell, the maximum of the electric field intensity can be compared with the maximum of the double-stub unit cell when the electric field direction is along the y-axis, but the area of resonance generated by the single-stub unit cell is smaller than the area of the double-stub unit cell. Moreover, the single-stub unit cell cannot generate resonance of the same intensity for the electric field along the x-axis direction to the incidence of the electric field in the y-axis direction, which

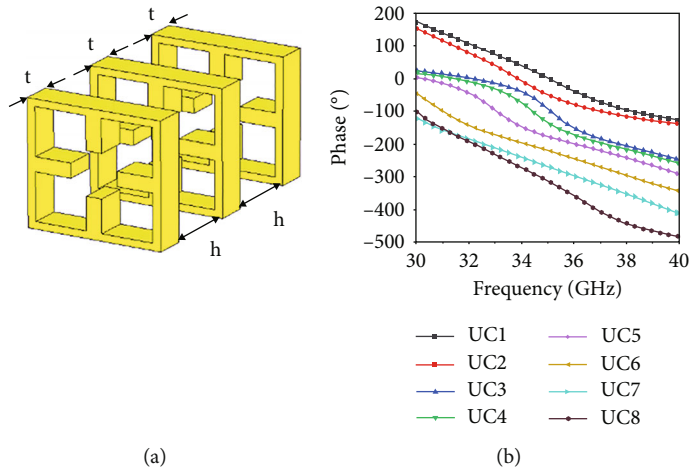

FIGURE 7: (a) Schematic of the proposed three metallic layers' unit cell. (b) Simulated transmission phase of the 3-bit three metallic layer unit cells with two pairs of orthogonal stubs.

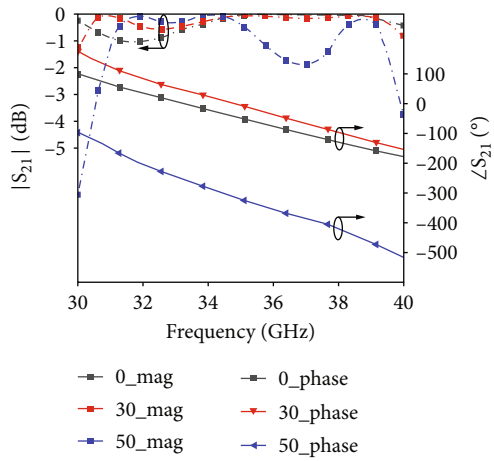

FIGURE 8: The simulated transmission coefficients (magnitude and phase) of the three metallic layers for various incident angles at 30 GHz-40 GHz.

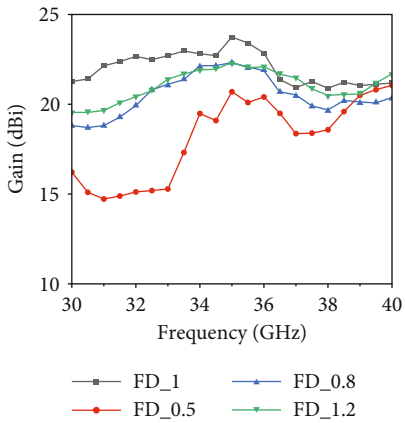

FIGURE 9: The simulated gain of TAs in a 0-degree direction with different F/D values at 30 GHz-40 GHz.

would result in the inability of the unit cell to perform CP wave transmission.

In Figure 5, the electric field shows the overall phase cycle from 0° to 270°. The arrows in Figure 5 indicate the direction of the electric field. Two pairs of orthogonal stubs are excited by the incident electric field. The maximum of the electric field switches on the orthogonal stubs with the phase cycle. The introduction of the orthogonal stubs makes the electric field move more smoothly at the edge of the metal-only unit cell, which can reduce the axial ratio of the unit cell [29]. Since circular polarization is composed of two mutually orthogonal line polarization waves and the symmetry design of the metal-only unit cell, the transmission mechanism of the unit cell for left- and right-handed circularly polarized waves is similar. Based on the combined action of the additional resonance between metallic layers and the resonance of the unit cell, the three-layer metal-only unit cell can achieve a 325° phase shift in the wideband range. The schematic of the proposed three-metallic-layer unit cell is shown in Figure 5(a). By changing the dimensions of L and D, we can get 3-bit unit cells with different phase responses. The specific dimensions corresponding to the eight different unit cells are shown in Table 1.

In Figure 6, the simulated transmission magnitudes of UC2 with different h values are shown. The unit cell obtains the transmission magnitude within -1 dB, when the height of the air gap is $h = 2.4$ mm. In the operating band, we have simulated different values of h, as shown in Figure 6; when h is equal to 2.4 mm, we can ensure that the transmission amplitude is less than -1 dB in the operating band range of 30 GHz-40 GHz of the unit cell. Other values will cause the transmission magnitude of the unit cell less than -1 dB at the edge of the operating frequency range. Thus, we choose the value of h with more stable performance in the operating bandwidth range. In Figure 7(b), we can find that the unit cell phase distribution near the center frequency is more uniform, but at the upper and lower frequencies, the cell phase distribution appears to merge phenomenon. The original design of the 3-bit unit cell to 2-bit unit cell design

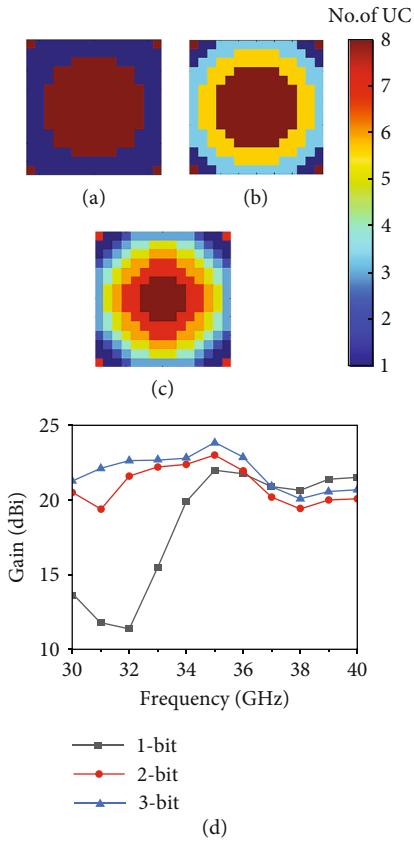

Figure 10: The phase quantization distribution of the TAs in broadside beam direction (a) 1 bit. (b) 2 bits. (c) 3 bits. (d) The gain in three quantified cases.

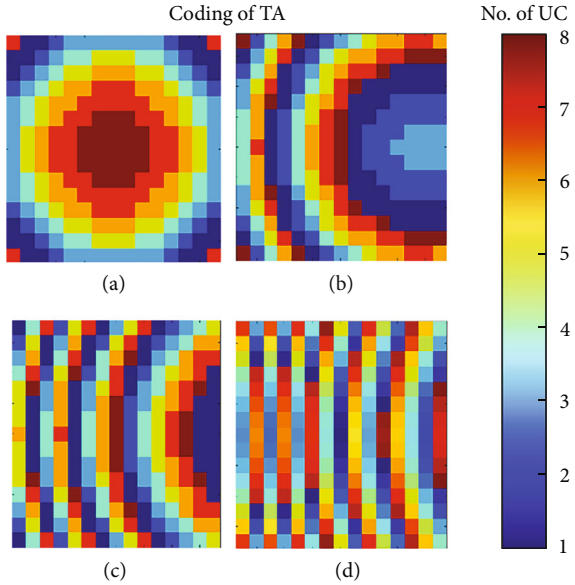

Figure 11: The 3-bit phase quantization distribution of the TAs in four beam directions at 35 GHz. (a) 0 degrees. (b) 15 degrees. (c) 30 degrees. (d) 50 degrees.

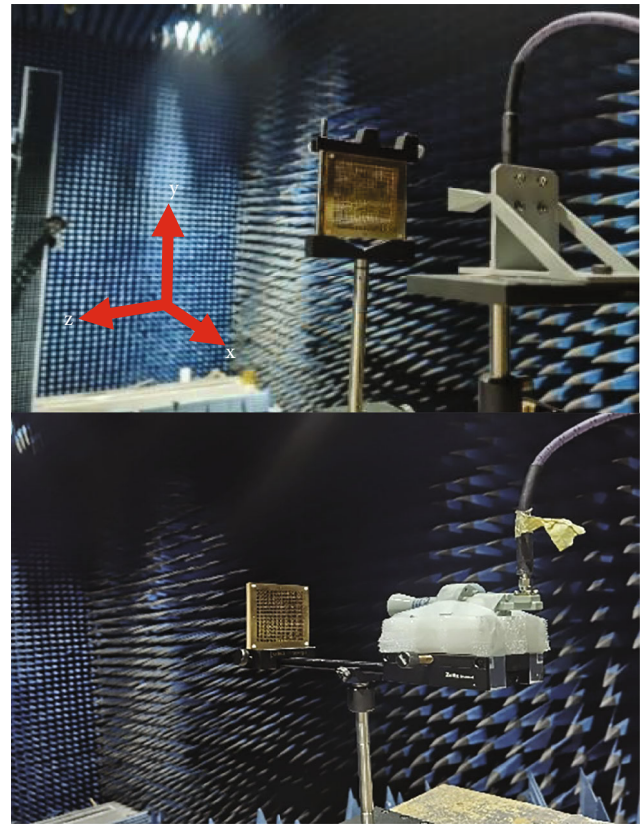

Figure 12: Photograph of the fabricated TA in the anechoic chamber.

transformation is bound to bring a certain amount of phase quantization error and gain attenuation at the upper and lower frequencies.

Figure 8 shows the transmission magnitude and phase at different incident angles from 30 GHz to 40 GHz. It can be seen that the magnitude and phase were kept stable in the incident angle range of 30°. Therefore, we should select a more appropriate focal diameter ratio to reduce the error and ensure the transmission performance of the TA.

3. Design of the Metal-Only Transmitarray Antenna

Four TAs with different main beam directions have been proposed. They can be excited by linearly polarized pyramidal horns or circularly polarized horns. In Figure 9, we have simulated the TA with different F/D values in direction of 0°. In the case of a F/D value of 1, TA can maintain a stable gain in the operating band, and the gain is higher compared with other F/D values. The focal length F is 90.2 mm, and F/D is equal to 1, ensuring the maximum gain at the central frequency of 35 GHz. The TAs are arranged by using the abovementioned 3-bit unit cells. To obtain a high-gain beam, the continuous phase distribution is phase quantized with a 3-bit metal-only unit cell according to the spatial distance from the phase center to different positions of the TA. In Figure 10, we performed 1-bit, 2-bit, and 3-bit phase quantization for the 15×15 TA and simulated the TA for

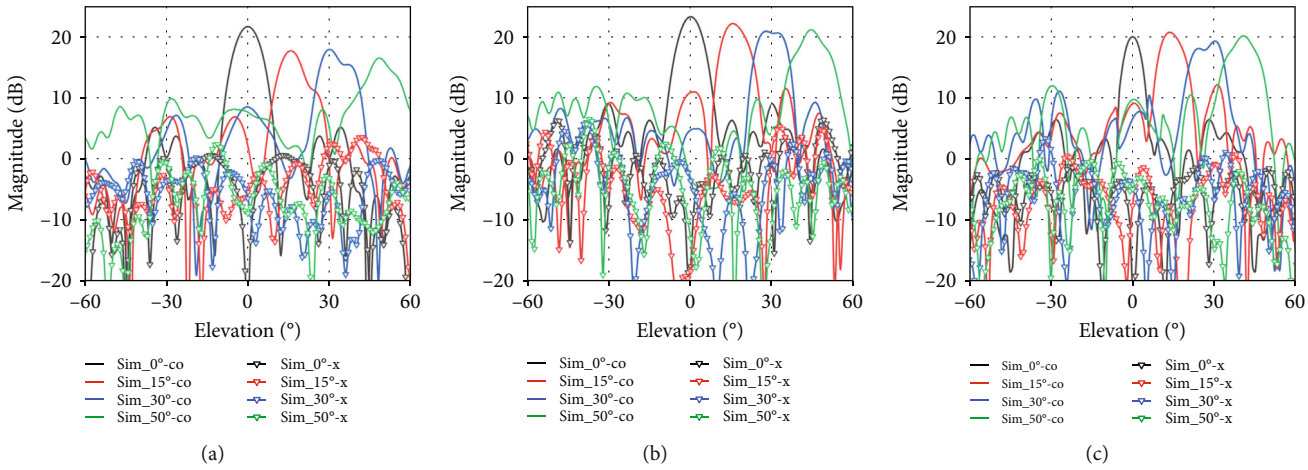

FIGURE 13: Simulated copolar and cross-polar radiation patterns of the four TA panels with LP feed of E-plane at (a) 30 GHz, (b) 35 GHz, and (c) 40 GHz.

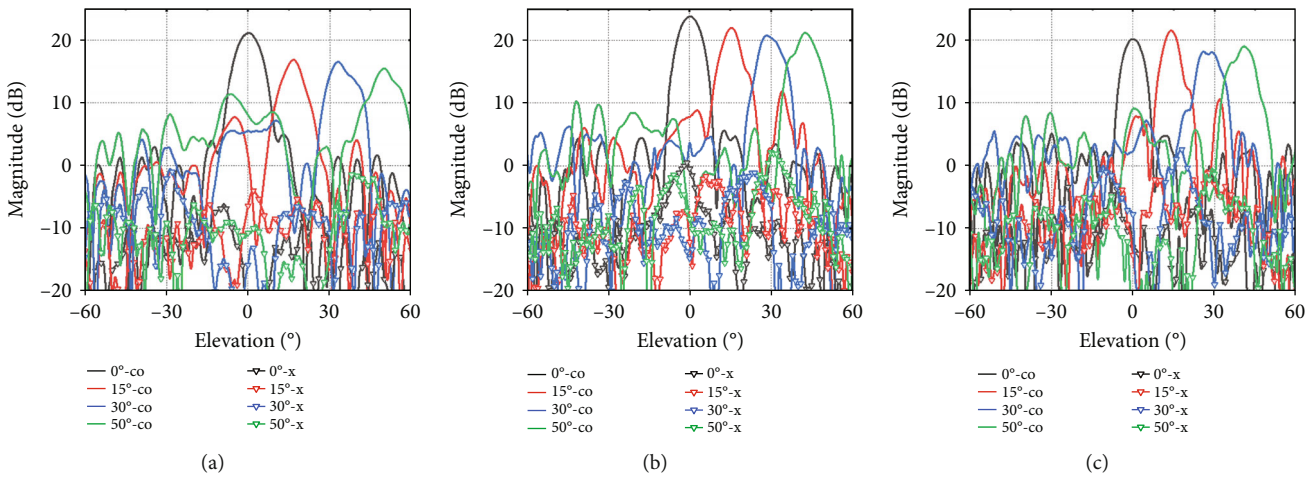

FIGURE 14: Measured copolar and cross-polar radiation patterns of the four TA panels with LP feed of E-plane at (a) 30 GHz, (b) 35 GHz, and (c) 40 GHz.

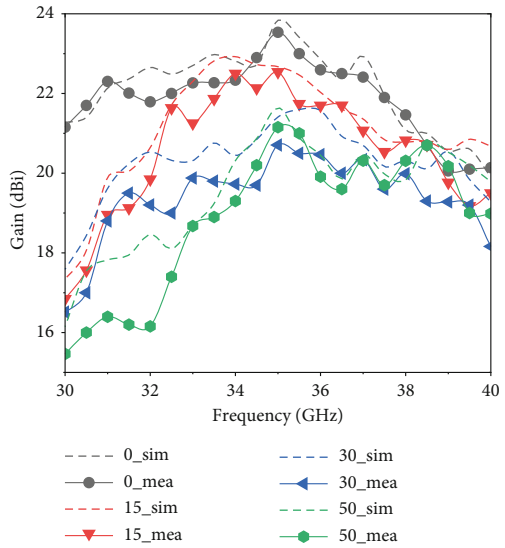

FIGURE 15: The simulated and measured gain of the TAs with LP feed for different main beam directions.

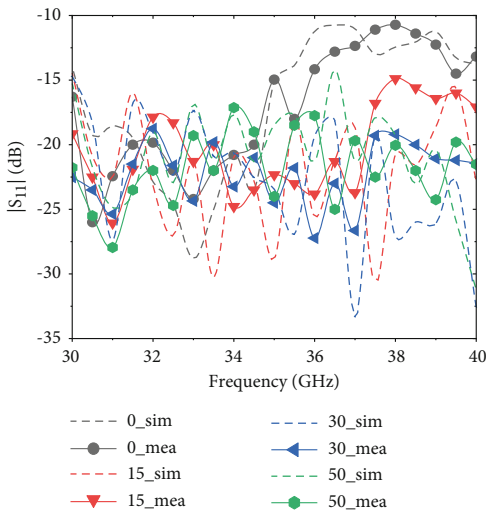

FIGURE 16: The simulated and measured S_{11} of the TAs with LP feed for different main beam directions.

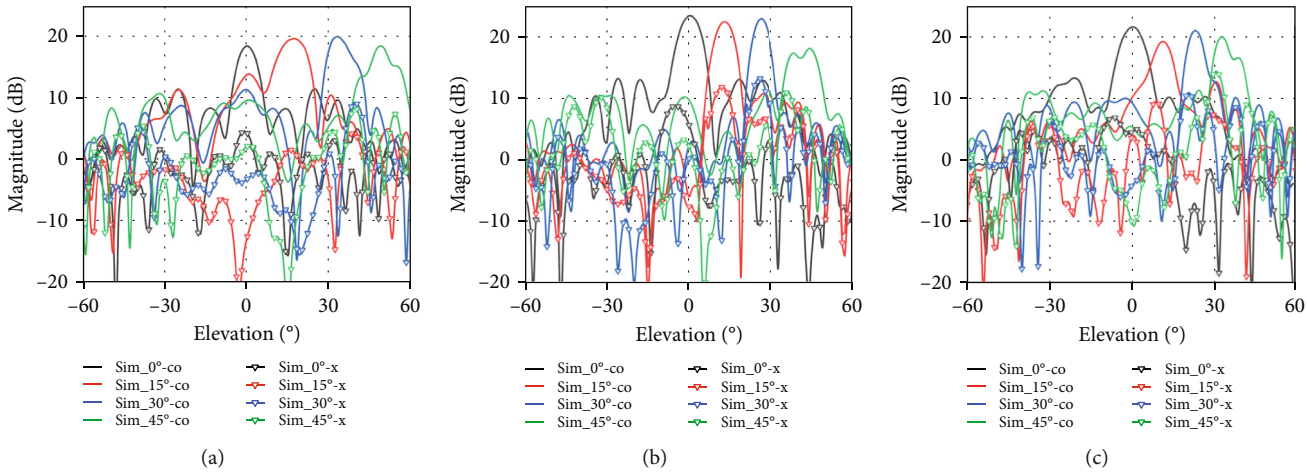

FIGURE 17: Simulated copolar and cross-polar radiation patterns of the four TA panels with LHCP feed of E-plane at (a) 30 GHz, (b) 35 GHz, and (c) 40 GHz.

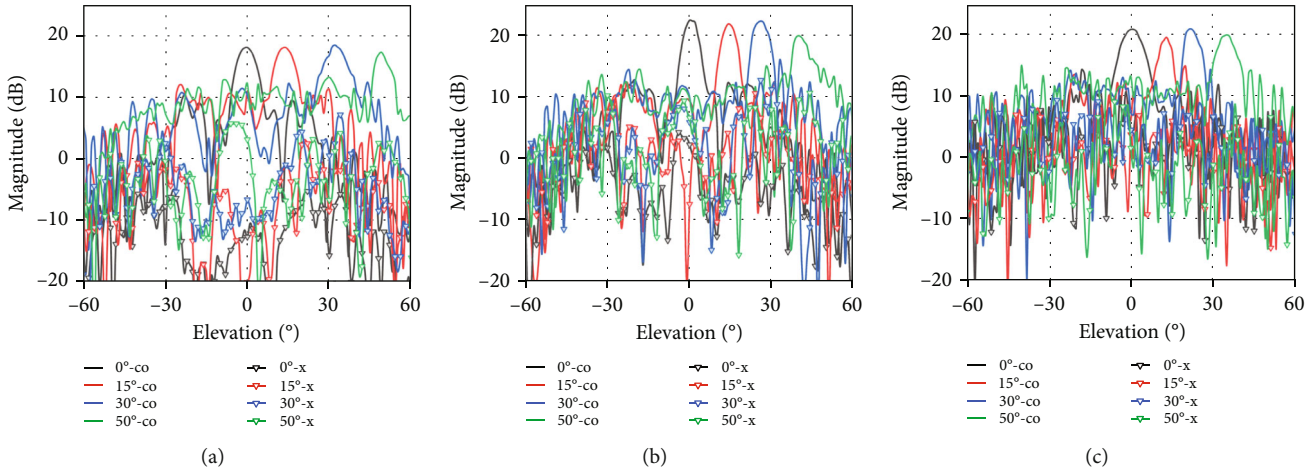

FIGURE 18: Measured copolar and cross-polar radiation patterns of the four TA panels with LHCP feed of E-plane at (a) 30 GHz, (b) 35 GHz, and (c) 40 GHz.

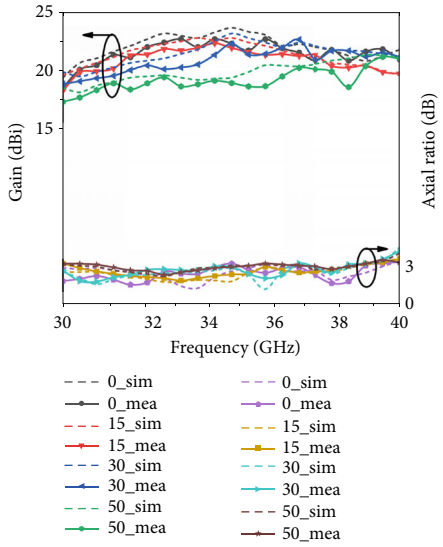

FIGURE 19: The simulated and measured gain and the axial ratio of the four TAs with LHCP feed.

the three quantization cases. With the quantized bit increasing, it can be seen that the overall gain of TA also gradually increases in Figure 10(d). Hence, we choose the 3-bit phase quantization to get a better 3 dB bandwidth performance.

Each unit cell can provide the appropriate phase shift to compensate for the spatial delay between the phase center of the feed source and the array. According to (1), the phase of the mnth unit cell ϕ_{mn} can be obtained by [30]:

$$\phi_{mn} = k_0(r_{mn} - (x_{mn}\sin\theta\cos\varphi + y_{mn}\sin\theta\sin\varphi)) + \varphi_0, \quad (1)$$

where k_0 is the propagation constant in the free space, r_{mn} is the distance from the mnth unit cell to the phase center of the horn feed, (x_{mn}, y_{mn}) is the distance between the mnth unit cells. The coding of TAs is calculated, as shown in Figure 11. Based on the coding of the TAs, a square aperture TA of $7.5^*\lambda_0$ with the metal-only unit cell is simulated. It includes 225 UCs. The polarization of the pyramidal horn is along the y-axis. Its operating frequency is from

Table 2: Comparison of the metal-only TA performance.

Ref.	Feed polarization	f_0 (GHz)	Gain (dBi)	3 dB BW (%)	Aperture efficiency (%)
[20]	LP	11.3	23.7	9.6	16
[25]	LP	29.5	29.9	11	50.9
[26]	LP	10	21.6	30.2	23.5
[27]	LP	8.5	16.3	24.3	47.6
[31]	RHCP	9.375	—	—	—
[32]	LP & dual CP	12.5	16	7.17	11.21
This work	LP & dual CP	35	23.53(LP)/22.3(LHCP)	28.5	31.7

Table 3: Gain loss analysis for broadside beam with LP feed.

Ideal directivity	28.5 dBi
Assembling loss	1.15 dB
Taper loss	0.75 dB
Aperture efficiency	31.7%
Spillover loss	1.27 dB
Quantization loss	0.1 dB
TA insertion loss	1.7 dB
Measured gain	23.53 dB

26.5 to 40 GHz, covering the entire working frequency band of the TA.

4. Fabrication and Measurement

To verify this design, the configuration of the proposed TA was fabricated and assembled. The metallic layers were processed by wire electrical discharge machining-low speed (WEDM-LS), and the fabrication accuracy can reach within $\pm 5\,\mu$m. One-millimeter-thick brass sheets were adopted. The area of the metallic layer is up to 79.5 mm × 79.5 mm. The spacer as an air gap is made of photopolymer with a size of 79.5 mm × 79.5 mm × 2.4 mm. We assembled the three-metal layer and the two-spacer layer. The measurement was conducted in an anechoic chamber, and the complete experimental far-field testing setup is shown in Figure 12.

The simulated and measured main beam direction results with LP feed are depicted in Figures 13 and 14, which show the main beam direction from 30 to 40 GHz at E-plane. Since the phase quantization strategy of the overall array is at the central operating frequency of 35 GHz, the main beam direction, sidelobe, and cross-polarization of the TA can achieve the best performance at the central operating frequency. The sidelobe and cross-polarization levels are kept below –10 and –20 dB in the main beam direction of 0°~50°. Similarly, by adopting a similar phase quantization strategy, the main beam direction of -50°~0°can also be realized. The simulated and measured radiation patterns in co- and cross-polarization at E-plane have a good consistency.

Under the analysis of the previous 3-bit unit cell transmission amplitude, the 3-bit unit cell at the upper and lower edge of the frequency of the phase will appear to the 2-bit unit cell conversion trend. The overall TA design operating frequency at 35 GHz will lead to quantization error out of the central frequency. The appearance of the radiation pattern away from the central frequency is mainly expressed in the drop of the gain and the rise of the sidelobe.

In Figures 15 and 16, we compared the gain and S_{11} of TAs for the simulated and measured results, respectively. The TAs are covering the main beam direction in the range of 0°~50°. Under different main beam direction cases, the 3 dB bandwidth of four different TAs is 22.2%-28.5%. The reflection coefficients of the TAs are below -10 dB. Its measured peak gain is 23.53 dB at 35 GHz, and its peak aperture efficiency is about 31.7%. It is evident that the measured results are in good agreement with the simulated results.

We also conducted the simulation and the measurement on circular polarization excitation of the four proposed TAs (0 degrees, 15 degrees, 30 degrees, and 50 degrees), using the left-hand circular polarization excitation. The copolar and cross-polar radiation patterns of the TAs at 30 GHz, 35 GHz, and 40 GHz are shown in Figures 17 and 18.

We also compared the gain and axial ratio under simulation and measurement with LHCP horn excitation. Due to the symmetry of the overall structure of the TA structure, the results of the LHCP excitation and the RHCP excitation are approximate, so only one feeding excitation is shown in Figure 19. With LHCP excitation, the measured peak gain of the 0-degree TA is 22.3 dB at 35 GHz.

The comparison of the proposed TA with the previous research is given in Table 2. The feed polarization in this prototype is more diverse, and the circular polarization excitation method can be better applied to SATCOM. Compared with [20], the central frequency of this letter is higher, which is more suitable for millimeter-wave applications. Meanwhile, this design makes full use of millimeter wave spectrum resources, compared with the metal-only TA operating in Ka-band, which are presented in [25]. The thickness of the metallic layers in this design is greater than that of the previous structure, but the profile of the array is still lower than most of the reported research [20, 26, 27], which not only maintains the overall mechanical robustness but also ensures lower assembly complexity and higher integration. Compared with the existing metal-only circularly polarized TA [31, 32], the structure of this design has a better simplicity and obvious advantages in 3 dB bandwidth and aperture efficiency. The gain loss analysis for broadside beam TA (0 degrees) with LP feed is calculated [30]. The

power budget estimation is summarized in Table 3. The spillover loss is 1.27 dB, and the insertion loss is 1.7 dB. The assembling loss refers to the gain drop introduced by the spacers and screws (tooling). We simulated the results with and without tooling. Accordingly, the assembling loss is 1.15 dB.

5. Conclusion

This paper demonstrates a wideband multipolarization metal-only TA based on the 3-bit unit cell. The metal-only unit cell comprises three metallic layers and two air gaps without any substrates. The proposed metal-only unit cell is easy to process and has high stability, so it can be widely used in complex space electromagnetic environments. Furthermore, the proposed TA can be excited by line polarization and circular polarization excitation, which is an indispensable condition for the application of SATCOM. The 0-degree TA achieves a measured gain of 23.53 dB and has 28.5% in 3 dB bandwidth. The measured results are consistent with the simulated results. The proposed design can be expanded to a higher-frequency millimeter wave band and fully utilized in wideband SATCOM applications.

Data Availability

The data that support the findings of this study are available from the corresponding author upon reasonable request.

Conflicts of Interest

The authors declare that they have no conflicts of interest.

Acknowledgments

This work was supported by the China Postdoctoral Science Foundation Grant No. 2022 M720654.

References

[1] J. Liu, Y. Shi, L. Zhao, Y. Cao, W. Sun, and N. Kato, "Joint placement of controllers and gateways in SDN-enabled 5G-satellite integrated network," *IEEE Journal on Selected Areas in Communications*, vol. 36, no. 2, pp. 221–232, 2018.

[2] J. A. del Peral-Rosado, R. Raulefs, J. A. Lopez-Salcedo, and G. Seco-Granados, "Survey of cellular mobile radio localization methods: from 1G to 5G," *IEEE Communications Surveys & Tutorials*, vol. 20, no. 2, pp. 1124–1148, 2018.

[3] A. Guidotti, A. Vanelli-Coralli, M. Conti et al., "Architectures and key technical challenges for 5G systems incorporating satellites," *IEEE Transactions on Vehicular Technology*, vol. 68, no. 3, pp. 2624–2639, 2019.

[4] V. Joroughi, L. K. Alminde, and E. Cruz, "5G satellite communications services through constellation of LEO satellites," in *Ad-Hoc, Mobile, and Wireless Networks*, pp. 543–548, Springer, 2019.

[5] M. Jia, X. Gu, Q. Guo, W. Xiang, and N. Zhang, "Broadband hybrid satellite-terrestrial communication systems based on cognitive radio toward 5G," *IEEE Wireless Communications*, vol. 23, no. 6, pp. 96–106, 2016.

[6] A. D. Panagopoulos, P.-D. M. Arapoglou, and P. G. Cottis, "Satellite communications at Ku, Ka, and V bands: propagation impairments and mitigation techniques," *IEEE Communications Surveys & Tutorials*, vol. 6, no. 3, pp. 2–14, 2004.

[7] K. W. Lam, S. W. Kwok, Y. Hwang, and T. K. Lo, "Implementation of transmitarray antenna concept by using aperture-coupled microstrip patches," in *Proceedings of 1997 Asia-Pacific Microwave Conference*, pp. 433–436, Hong Kong, 1997.

[8] N. Yu, P. Genevet, M. A. Kats et al., "Light propagation with phase discontinuities: generalized laws of reflection and refraction," *Science*, vol. 334, no. 6054, pp. 333–337, 2011.

[9] C. Pfeiffer and A. Grbic, "Millimeter-wave transmitarrays for wavefront and polarization control," *IEEE Transactions on Microwave Theory and Techniques*, vol. 61, no. 12, pp. 4407–4417, 2013.

[10] L. Gao, Q. Cheng, J. Yang et al., "Broadband diffusion of terahertz waves by multi-bit coding metasurfaces," *Light: Science & Applications*, vol. 4, no. 9, article e324, 2015.

[11] L. Wu, H. F. Ma, Y. Gou et al., "High-transmission ultrathin Huygens' metasurface with 360° phase control by using double-layer transmitarray elements," *Physical Review Applied*, vol. 12, no. 2, article 024012, 2019.

[12] Y. Liu, A. Zhang, Z. Xu, S. Xia, and H. Shi, "Wideband and low-profile transmitarray antenna using transmissive metasurface," *Journal of Applied Physics*, vol. 125, no. 4, article 045103, 2019.

[13] X. Yang, Y. Zhou, L. Xing, and Y. Zhao, "A wideband and low-profile transmitarray antenna using different types of unit-cells," *Microwave and Optical Technology Letters*, vol. 61, no. 6, pp. 1584–1589, 2019.

[14] B. Liu and C. Song, "High gain transmitarray antenna based on ultra-thin metasurface," *International Journal of RF and Microwave Computer-Aided Engineering*, vol. 29, no. 5, article e21655, 2019.

[15] X. Zhong, Z. Lei, M. Dong, and Q. Xiao, "A low-profile circularly polarized transmitarray antenna using rotated cross dipole elements," *International Journal of RF and Microwave Computer-Aided Engineering*, vol. 30, no. 3, article e22082, 2020.

[16] H. Zhu, L. Guo, and W. Feng, "A low-profile transmitarray antenna using square patch elements with cross dipole slots and vias," *International Journal of RF and Microwave Computer-Aided Engineering*, vol. 30, no. 4, article e22106, 2020.

[17] K. Narayanasamy, G. N. A. Mohammed, K. Savarimuthu, R. Sivasamy, and M. Kanagasabai, "A comprehensive analysis on the state-of-the-art developments in reflectarray, transmitarray, and transmit-reflectarray antennas," *International Journal of RF and Microwave Computer-Aided Engineering*, vol. 30, no. 9, article e22272, 2020.

[18] Y. Liu, Z. Ren, Y. Shu et al., "Broadband, large-numerical-aperture and high-efficiency microwave metalens by using a double-layer transmissive metasurface," *Applied Physics Express*, vol. 15, no. 1, article 014003, 2022.

[19] M. O. Bagheri, H. R. Hassani, and B. Rahmati, "Dual-band, dual-polarised metallic slot transmitarray antenna," *IET Microwaves, Antennas & Propagation*, vol. 11, no. 3, pp. 402–409, 2017.

[20] A. H. Abdelrahman, A. Z. Elsherbeni, and F. Yang, "Transmitarray antenna design using cross-slot elements with no

dielectric substrate," *IEEE Antennas and Wireless Propagation Letters*, vol. 13, pp. 177–180, 2014.

[21] B. Rahmati and H. R. Hassani, "High-efficient wideband slot transmitarray antenna," *IEEE Transactions on Antennas and Propagation.*, vol. 63, no. 11, pp. 5149–5155, 2015.

[22] R. Wu, Y. Li, W. Wu, C. Shi, and T. Cui, "High-gain dual-band transmitarray," *IEEE Transactions on Antennas and Propagation*, vol. 65, no. 7, pp. 3481–3488, 2017.

[23] S. H. Ramazannia Tuloti, P. Rezaei, and H. F. Tavakkol, "High-efficient wideband transmitarray antenna," *IEEE Antennas and Wireless Propagation Letters*, vol. 17, no. 5, pp. 817–820, 2018.

[24] Z. Liu, S. Liu, X. Kong, Z. Huang, X. Zhao, and J. Liu, "Gain enhancement of circularly polarized antenna with dual-polarization conversion transmitarray," *International Journal of RF and Microwave Computer-Aided Engineering*, vol. 29, no. 6, article e21669, 2019.

[25] K. T. Pham, A. Clemente, E. Fourn, F. Diaby, L. Dussopt, and R. Sauleau, "Low-cost metal-only transmitarray antennas at Ka-band," *IEEE Antennas and Wireless Propagation Letters*, vol. 18, no. 6, pp. 1243–1247, 2019.

[26] G. Chen, Y. Jiao, and G. Zhao, "Novel wideband metal-only transmitarray antenna based on 1-bit polarization rotation element," *International Journal of RF and Microwave Computer-Aided Engineering*, vol. 30, no. 11, 2020.

[27] W. Hu, J. Dong, Q. Luo et al., "A wideband metal-only transmitarray with two-layer configuration," *IEEE Antennas and Wireless Propagation Letters*, vol. 20, no. 7, pp. 1347–1351, 2021.

[28] L. He, J. F. Lv, C. Ding et al., "All-metallic near-field convergent lens design using cross-Jerusalem-slot elements," *International Journal of RF and Microwave Computer-Aided Engineering*, vol. 32, no. 3, article e23021, 2022.

[29] K. Q. Henderson and N. Ghalichechian, "Circular-polarized metal-only reflectarray with multi-slot elements," *IEEE Transactions on Antennas and Propagation*, vol. 68, no. 9, pp. 6695–6703, 2020.

[30] A. H. Abdelrahman, F. Yang, A. Z. Elsherbeni et al., "Introduction," in *Analysis and Design Transmitarray Antenna*, pp. 1–6, Springer, 2017.

[31] X. Zhao, C. Yuan, L. Liu et al., "All-metal beam steering lens antenna for high power microwave applications," *IEEE Transactions on Antennas and Propagation*, vol. 65, pp. 1–7344, 2017.

[32] F. Ahmed, M. U. Afzal, T. Hayat, K. P. Esselle, and D. N. Thalakotuna, "A near-field meta-steering antenna system with fully metallic metasurfaces," *IEEE Transactions on Antennas and Propagation*, vol. 70, no. 11, pp. 10062–10075, 2022.